Direct engagement of the PI3K pathway by mutant KIT dominates oncogenic signaling in gastrointestinal stromal tumor

Benedikt Bosbach[a,b,1,2], Ferdinand Rossi[a,c,1], Yasemin Yozgat[a,3], Jennifer Loo[c], Jennifer Q. Zhang[c], Georgina Berrozpe[d], Katherine Warpinski[d], Imke Ehlers[a,4], Darren Veach[e], Andrew Kwok[c], Katia Manova[a], Cristina R. Antonescu[f], Ronald P. DeMatteo[c,5], and Peter Besmer[a,5]

[a]Developmental Biology Program, Memorial Sloan Kettering Cancer Center, New York, NY 10065; [b]Cancer Biology and Genetics Program, Memorial Sloan Kettering Cancer Center, New York, NY 10065; [c]Department of Surgery, Memorial Sloan Kettering Cancer Center, New York, NY 10065; [d]Molecular Biology Program, Memorial Sloan Kettering Cancer Center, New York, NY 10065; [e]Department of Radiology, Memorial Sloan Kettering Cancer Center, New York, NY 10065; and [f]Department of Pathology, Memorial Sloan Kettering Cancer Center, New York, NY 10065

Edited by Peter K. Vogt, The Scripps Research Institute, La Jolla, CA, and approved August 25, 2017 (received for review June 28, 2017)

Gastrointestinal stromal tumors (GISTs) predominantly harbor activating mutations in the receptor tyrosine kinase KIT. To genetically dissect in vivo the requirement of different signal transduction pathways emanating from KIT for tumorigenesis, the oncogenic $Kit^{V558\Delta}$ mutation was combined with point mutations abrogating specific phosphorylation sites on KIT. Compared with single-mutant $Kit^{V558\Delta/+}$ mice, double-mutant $Kit^{V558\Delta;Y567F/Y567F}$ knock-in mice lacking the SRC family kinase-binding site on KIT (pY567) exhibited attenuated MAPK signaling and tumor growth. Surprisingly, abrogation of the PI3K-binding site (pY719) in $Kit^{V558\Delta;Y719F/Y719F}$ mice prevented GIST development, although the interstitial cells of Cajal (ICC), the cells of origin of GIST, were normal. Pharmacologic inhibition of the PI3K pathway in tumor-bearing $Kit^{V558\Delta/+}$ mice with the dual PI3K/mTOR inhibitor voxtalisib, the pan-PI3K inhibitor pilaralisib, and the PI3K-alpha–restricted inhibitor alpelisib each diminished tumor proliferation. The addition of the MEK inhibitor PD-325901 or binimetinib further decreased downstream KIT signaling. Moreover, combining PI3K and MEK inhibition was effective against imatinib-resistant $Kit^{V558\Delta;T669I/+}$ tumors.

GIST | Kit | PI3K | mouse

Targeted therapies have revolutionized cancer care, but the rapidity with which resistance to single-agent treatments develops has unsettled the field. Often the mechanism of resistance is further mutation of the originally targeted oncogene, as occurs with $ABL1^{T315I}$, KIT^{T670I}, $EGFR^{T790M}$, and ALK^{L1196M}. Thus, key protumorigenic signals must be emanating from these "oncogenic drivers." To date, however, the contribution of individual signal transduction sites on oncogenic drivers has not been dissected using endogenously encoded oncogenes in fully immunocompetent, genetically engineered models of cancer.

Gastrointestinal stromal tumors (GISTs) derive from mesenchymal pacemaker cells of the gastrointestinal tract known as interstitial cells of Cajal (ICCs) or their progenitors (1, 2). The receptor tyrosine kinase KIT is essential for the development of ICCs, and KIT-activating mutations are detected in the majority of GISTs (1, 3, 4). The tyrosine kinase inhibitor imatinib mesylate is approved for first-line treatment of advanced GIST. as well as for adjuvant treatment following resection of KIT-positive GIST (5). Despite the early clinical success of imatinib for the treatment of GIST, it is rarely curative, with the main outcome being partial response or stable disease, requiring lifelong therapy (6). In addition, imatinib resistance frequently arises from second-site mutations in *Kit* (7, 8).

We previously generated a mouse model of GIST that carries the $Kit^{V558\Delta}$ mutation, which is prototypical for *Kit* exon 11 mutations found in both spontaneous and familial GIST (9, 10). We also engineered imatinib-resistant $Kit^{V558\Delta;T669I/+}$ mice that model the human "gatekeeper mutation" Kit^{T670I} (7, 8, 11). Both mouse models develop gastric and colonic ICC hyperplasia and cecal GIST by histology and aberrant activation of SRC family kinase (SFK), PI3-kinase (PI3K)/AKT/S6, STAT3, and MAPK/ERK signal transduction pathways indistinguishable from human GIST (10–13). While these findings confirm the central and persistent role of KIT in the pathogenesis of GIST, they also highlight the need to identify other targets to improve clinical outcomes per se and provide the means to prevent or overcome the emergence of resistant clones. As aberrant KIT signaling is essential for most GISTs, we aimed to identify the proximal downstream targets critical for tumor development and/or maintenance.

Kit gain-of-function mutations are also found in neoplasms of the hematopoietic system, such as in mast cells and myeloid cells. In contrast to Kit mutations in GIST, which typically are weak gain-of-function mutations, *Kit* gain-of-function mutations in the hematopoietic system are strong mutations typically arising in the

Significance

Oncogenic receptor tyrosine kinases (RTKs) are important drug targets in the clinical setting. While RTK inhibitors have become important tools in the clinic, as has been demonstrated with chronic myelogenous leukemia and gastrointestinal stromal tumors (GIST), drug resistance invariably develops. The tools and rationale for the treatment of RTK drug resistance are limited, and success is of short duration. The identification of secondary intracellular drug targets is thus of critical importance. By using new Kit-GIST mouse models in which specific Kit signaling cascades are inhibited, we show the importance of PI3 kinase signaling in tumor development, as well as the utility of PI3 kinase inhibition in the treatment of primary and imatinib-resistant GIST. These studies provide a rationale for targeting dominant molecular pathways in tumors driven by oncogenic kinases.

Author contributions: B.B., F.R., G.B., K.M., C.R.A., R.P.D., and P.B. designed research; B.B., F.R., Y.Y., J.L., J.Q.Z., G.B., K.W., I.E., A.K., and C.R.A. performed research; D.V. contributed new reagents/analytic tools; B.B., F.R., Y.Y., J.L., G.B., I.E., D.V., K.M., C.R.A., R.P.D., and P.B. analyzed data; and B.B., F.R., R.P.D., and P.B. wrote the paper.

The authors declare no conflict of interest.

This article is a PNAS Direct Submission.

[1]B.B. and F.R. contributed equally to this work.

[2]Present address: Oncology Research Unit, Pfizer Worldwide Research & Development, Pearl River, NY 10965.

[3]Present address: Molecular Biology, Genetics and Bioengineering Program, Faculty of Engineering and Natural Sciences, Sabanci University, Istanbul, Turkey and Regenerative and Restorative Medicine Research Center, Istanbul Medipol University, Istanbul, Turkey 34956.

[4]Present address: Office of Technology Development, Memorial Sloan Kettering Cancer Center, New York, NY 10065.

[5]To whom correspondence may be addressed. Email: dematter@mskcc.org or p-besmer@ski.mskcc.org.

This article contains supporting information online at www.pnas.org/lookup/suppl/doi:10.1073/pnas.1711449114/-/DCSupplemental.

activation loop of the Kit kinase. This appears to be the result of the activation by KIT of a negative regulator of PI3K, SHIP1, in hematopoietic lineages. In agreement with this idea, SHIP1 loss-of-function mice display mast cell hyperplasia (14).

The receptor tyrosine kinase KIT contains 22 cytoplasmic tyrosine phosphorylation sites that are conserved between mouse and humans. Normal and oncogenic kinase activity of KIT results in their phosphorylation and the recruitment of a multitude of signal transducers to one or more of these docking sites on KIT. Depending on the cellular context, this signal transduction process elicits various biological responses, such as cell survival, proliferation, secretion, and migration. Two phosphorylation sites have been extensively studied in the nononcogenic setting. The phospho-Y567 (pY567) site, among other signaling intermediates, interacts with the SFKs (15, 16),

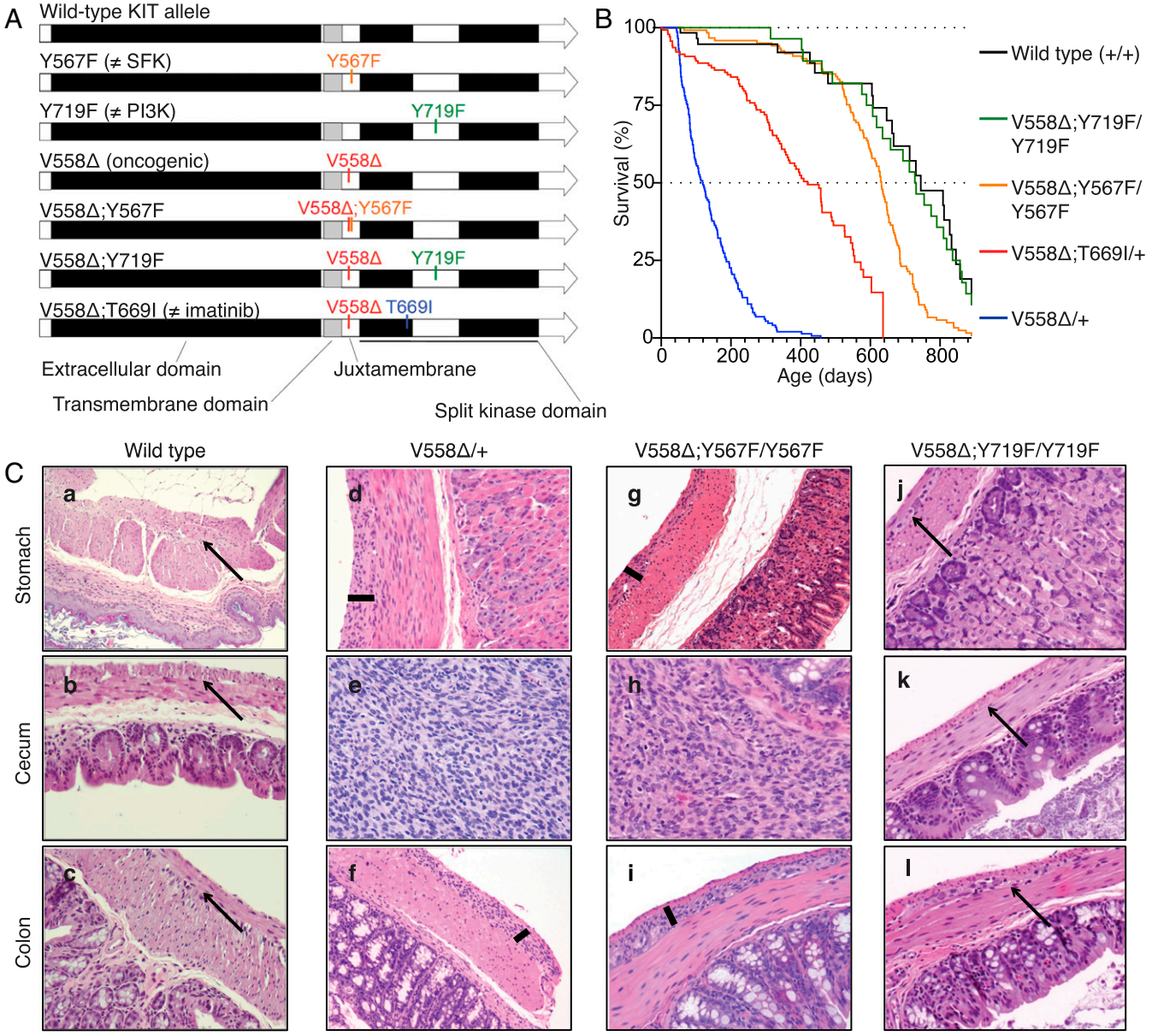

Fig. 1. Construction, survival, and histology of $Kit^{V558\Delta/+}$, $Kit^{V558\Delta;Y567F/Y567F}$, and $Kit^{V558\Delta;Y719F/Y719F}$ knock-in mice. (*A*) Schematic representation of targeted amino acids in the KIT protein. V558Δ, oncogenic mutation due to deletion of valine 558; V558Δ;T669I, double mutant containing the V558Δ and imatinib-resistant T669I mutations; V558Δ;Y567F, double mutant containing the V558Δ and Y567F mutations; V558Δ;Y719F, double mutant containing the V558Δ and Y719F mutations. Y567F, the docking site for the SFK tyrosine 567, is replaced by phenylalanine; Y719F, the docking site for the PI3K tyrosine 719, is replaced by phenylalanine. (*B*) Kaplan–Meier survival plot showing increased survival of $Kit^{V558\Delta;Y567F/Y567F}$ mice compared with fully signaling-competent $Kit^{V558\Delta/+}$ mice. Survival of $Kit^{V558\Delta;Y719F/Y719F}$ mice was indistinguishable from that of WT mice ($P = 0.791$). Survival of $Kit^{V558\Delta;Y567F/Y567F}$ mice was significantly different from that of $Kit^{V558\Delta;Y719F/Y719F}$ and WT mice ($P = 0.0003$ and 0.0004, respectively). All survival curve comparisons are based on the log-rank/Mantel–Cox method. Median survival: $Kit^{V558\Delta/+}$, 3 mo; $Kit^{V558\Delta;T669I/+}$, 14 mo; $Kit^{V558\Delta;Y567F/Y567F}$, 21 mo; $Kit^{V558\Delta;Y719F/Y719F}$, 28 mo; WT, 29 mo. Values for $Kit^{V558\Delta/+}$, $Kit^{V558\Delta;T669I/+}$, and WT mice are from ref. 11. $n \geq 43$ each; ticks indicate censored subjects. (*C*) Representative H&E-stained sections of FFPE samples of stomach, cecum, and colon from 3-mo-old mice. Arrows in *a–c* and *j–l* indicate the plane of normal myenteric plexus ICCs between the circular and longitudinal smooth muscle layers in WT and $Kit^{V558\Delta;Y719F/Y719F}$ mice. Bars in *d*, *f*, *g*, and *i* show hyperplastic extensions of this plane in gastric/colonic sections of $Kit^{V558\Delta/+}$ and $Kit^{V558\Delta;Y567F/Y567F}$ mice. The tumor lesions in the cecum of $Kit^{V558\Delta/+}$ (*e*) and $Kit^{V558\Delta;Y567F/Y567F}$ (*h*) mice exhibit typical GIST morphology with spindle-shaped/epithelioid tumor cells. The histology of $Kit^{V558\Delta;Y719F/Y719F}$ mice resembles that of WT mice. (Scale bar: 100 μm.) (Magnification, 10× in *a*, 20× in *b–l*). $n \geq 3$ animals each.

STAT3, and GRB2 (17), while phospho-Y719 (pY719) is the sole site on KIT for the recruitment of PI3K family members (18, 19).

We and others have studied the individual contributions of pY567 and pY719 to nononcogenic KIT signal transduction and, ultimately, cellular fate decisions using knock-in mouse models. Generally, KIT is essential for melanogenesis, hematopoiesis, and gametogenesis. $Kit^{Y567F/Y567F}$ mice specifically lacking the KIT^{Y567} phosphorylation site exhibit minor pigmentation changes and an age-dependent differentiation block in pro-B and pro-T cells, an erythroblast-intrinsic defect in stress erythropoiesis, but normal fertility (20–22). In contrast, $Kit^{Y719F/Y719F}$ mice lacking the KIT^{Y719} phosphorylation site have normal pigmentation and hematopoiesis, but males are sterile and females have defective ovarian follicle maturation (20, 23–25). Importantly, while KIT signaling is required in the ICC lineage, KIT-mediated SFK or PI3K signaling is dispensable, since both $Kit^{Y567F/Y567F}$ and $Kit^{Y719F/Y719F}$ mice show normal ICC development (4, 22, 26).

The individual downstream KIT signaling pathways required for the oncogenic transformation of ICCs and GIST maintenance are unknown, however. Identification of vital pathways could provide additional strategies to enhance the efficacy of existing therapies or to circumvent imatinib resistance. Thus, double–knock-in mouse models were generated combining the oncogenic $Kit^{V558\Delta}$ mutation with either the Kit^{Y567F} or the Kit^{Y719F} mutation in the endogenous *Kit* locus. Vital pathways identified with this approach were then targeted by specific inhibitors in both our imatinib-sensitive and imatinib-resistant mouse models to translate the genetic findings.

Results

PI3K, but Not SFK, Is Required for ICC Hyperplasia and GIST Oncogenesis. To dissect the in vivo contribution of individual signal transduction pathways emanating from oncogenic KIT, we genetically abrogated the SFK-binding site pY567 or the PI3-kinase binding site pY719 in the $KIT^{V558\Delta}$ oncoprotein by substituting the tyrosine to phenylalanine (Fig. 1*A* and Fig. S1). Heterozygosity for the $Kit^{V558\Delta}$ allele is sufficient to induce GIST development, while homozygosity causes perinatal lethality in mice (10). Because KIT dimerizes, homozygous phenylalanine substitutions were necessary to abrogate signaling from the specified tyrosines. $Kit^{V558\Delta;Y567F/Y567F}$ mice were viable and had longer survival than $Kit^{V558\Delta/+}$ and $Kit^{V558\Delta;T669I/+}$ mice, while $Kit^{V558\Delta;Y719F/Y719F}$ mice had a normal lifespan (Fig. 1*B*). $Kit^{V558\Delta;Y567F/Y567F}$ mice developed GIST in the cecum that was histologically similar to $Kit^{V558\Delta/+}$ tumors, but significantly smaller. $Kit^{V558\Delta;Y567F/Y567F}$ mice had less ICC hyperplasia in the stomach and colon (Fig. 1*C*, compare *d* and *f* with *g* and *i*) and less distention of the ileum from tumor obstruction, likely accounting for their longer survival (Fig. 2 *A*–*C*). Meanwhile, $Kit^{V558\Delta;Y719F/Y719F}$ mice ($n = 14$) up to 29 mo of age did not develop GIST. Histological

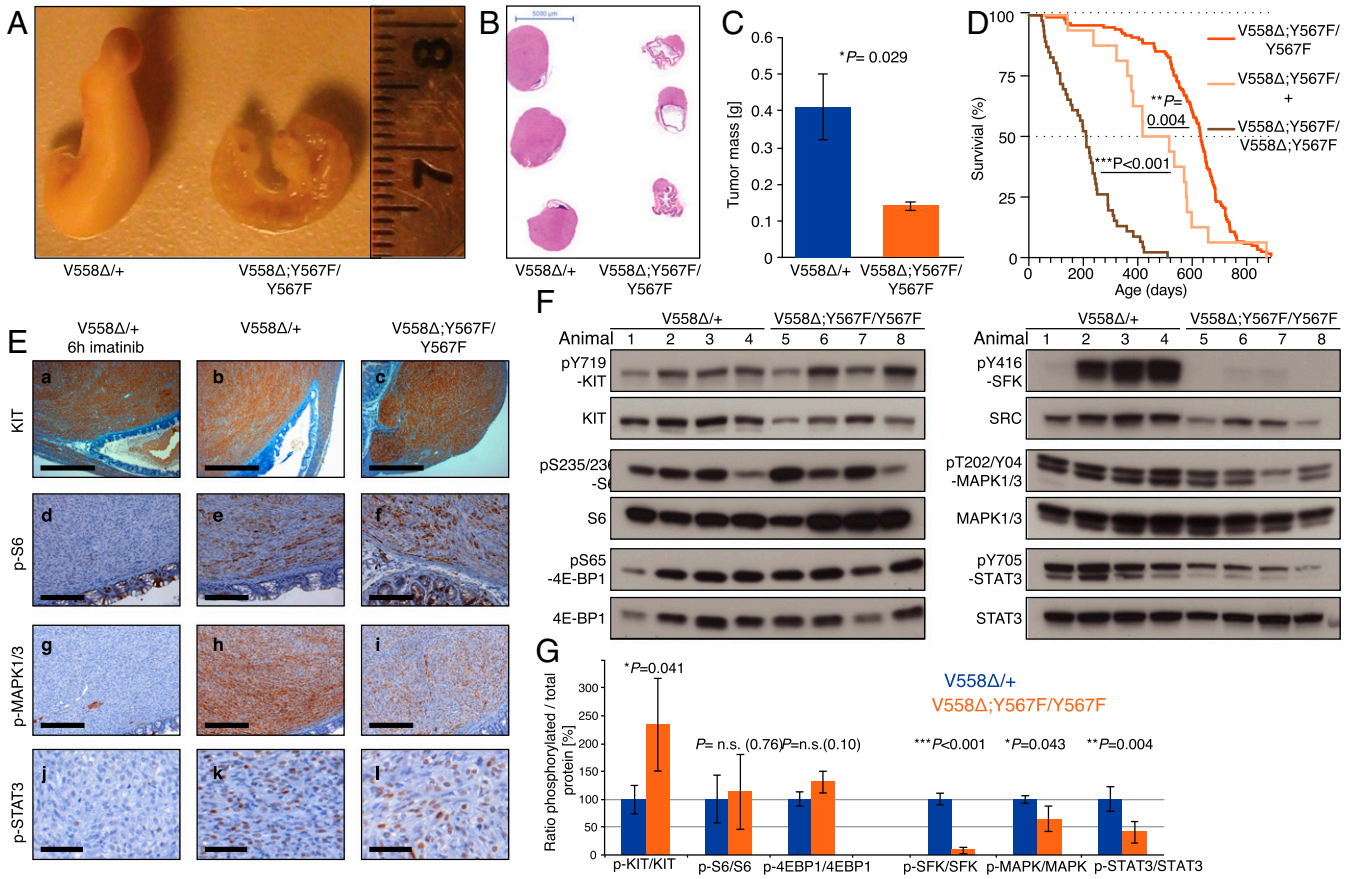

Fig. 2. Tumors from $Kit^{V558\Delta;Y567F/Y567F}$ mice are smaller and have lower MAPK and SFK pathway activation than tumors from $Kit^{V558\Delta/+}$ mice. (*A*) Representative gross cecal GISTs from 3-mo-old mice. (*B*) H&E staining of cross-sections of cecal GISTs from six mice. Note the unilateral tumor growth in relation to the cecal lumen in both genotypes and the compressed luminal diameter in $Kit^{V558\Delta/+}$ mice. (*C*) Tumor weights. $n = 3$–6. Error bars indicate mean ± SD. (*D*) Kaplan–Meier survival plot showing reduced survival of $Kit^{V558\Delta;Y567F/+}$ and $Kit^{V558\Delta;Y567F/V558\Delta;Y567F}$ mice compared with $Kit^{V558\Delta;Y567F/Y567F}$ mice. The median survival of $Kit^{V558\Delta;Y567F/+}$ and $Kit^{V558\Delta;Y567F/V558\Delta;Y567F}$ mice was 15 ($n = 16$) and 7 ($n = 46$) months, respectively, and the median survival of $Kit^{V558\Delta;Y567F/Y567F}$ was 21 mo ($n = 121$), as shown in Fig. 1. (*E*) Comparison of KIT expression and downstream signal transduction in GISTs of 3- to 4-mo-old mice by immunohistochemistry. (Scale bars: 500 μm in *a*–*c*, 200 μm in *d*–*i*, and 50 μm in *j*–*l*.) (*F* and G) Immunoblot analysis (*G*) and its quantification (*F*). n.s., nonsignificant. Scale is in arbitrary units (intensity of gray shading).

analysis revealed normal morphology of the stomach, cecum, and colon, with a normal density of ICCs in the myenteric plexus (Fig. 1*C*, *j–l*).

***Kit*$^{V558\Delta;Y567F/Y567F}$ Tumors Have Disrupted SFK Signaling.** While *Kit*$^{V558\Delta;Y567F/Y567F}$ mice had a smaller tumor and lived longer than *Kit*$^{V558\Delta}$ mice, *Kit*$^{V558\Delta;Y567F/+}$ mice with a wild-type (WT) *Kit* allele had a shorter lifespan than *Kit*$^{V558\Delta;Y567F/Y567F}$ mice, indicating that one dose of KIT^{Y567} signaling affected survival (Fig. 2*D*). Similarly, increasing the oncogenic dose in *Kit*$^{V558\Delta;Y567F/V558\Delta;Y567F}$ mice further reduced survival despite disruption of KIT^{Y567} signaling, confirming that signaling from other KIT tyrosines contributed to KIT signaling in GIST (Fig. 2*D*).

To verify the impaired SFK signaling in *Kit*$^{V558\Delta;Y567F/Y567F}$ tumors, we performed IHC and Western blot analysis. KIT staining was uniformly high in *Kit*$^{V558\Delta/+}$ and *Kit*$^{V558\Delta;Y567F/Y567F}$ tumors (Fig. 2*E*, *b* and *c*), while adjacent mucosal tissues, lymphoid follicles, and remaining intervening fibers of smooth muscles lacked KIT staining, as expected. Notably, *Kit*$^{V558\Delta;Y567F/Y567F}$ tumors were more heterogeneous, with remaining muscle fibers and fibrotic areas present. Importantly, S6 phosphorylation, a downstream indicator of PI3K activation, was equally high in *Kit*$^{V558\Delta/+}$ and *Kit*$^{V558\Delta;Y567F/Y567F}$ tumors (Fig. 2*E*, *e* and *f*). In contrast, phosphorylation of MAPK, and to a lesser extent STAT3, was diminished in *Kit*$^{V558\Delta;Y567F/Y567F}$ GIST lesions (Fig. 2*E*, *h*, *i*, *k*, and *l*). Imatinib treatment of *Kit*$^{V558\Delta/+}$ mice for 6 h reduced S6, MAPK1/3, and

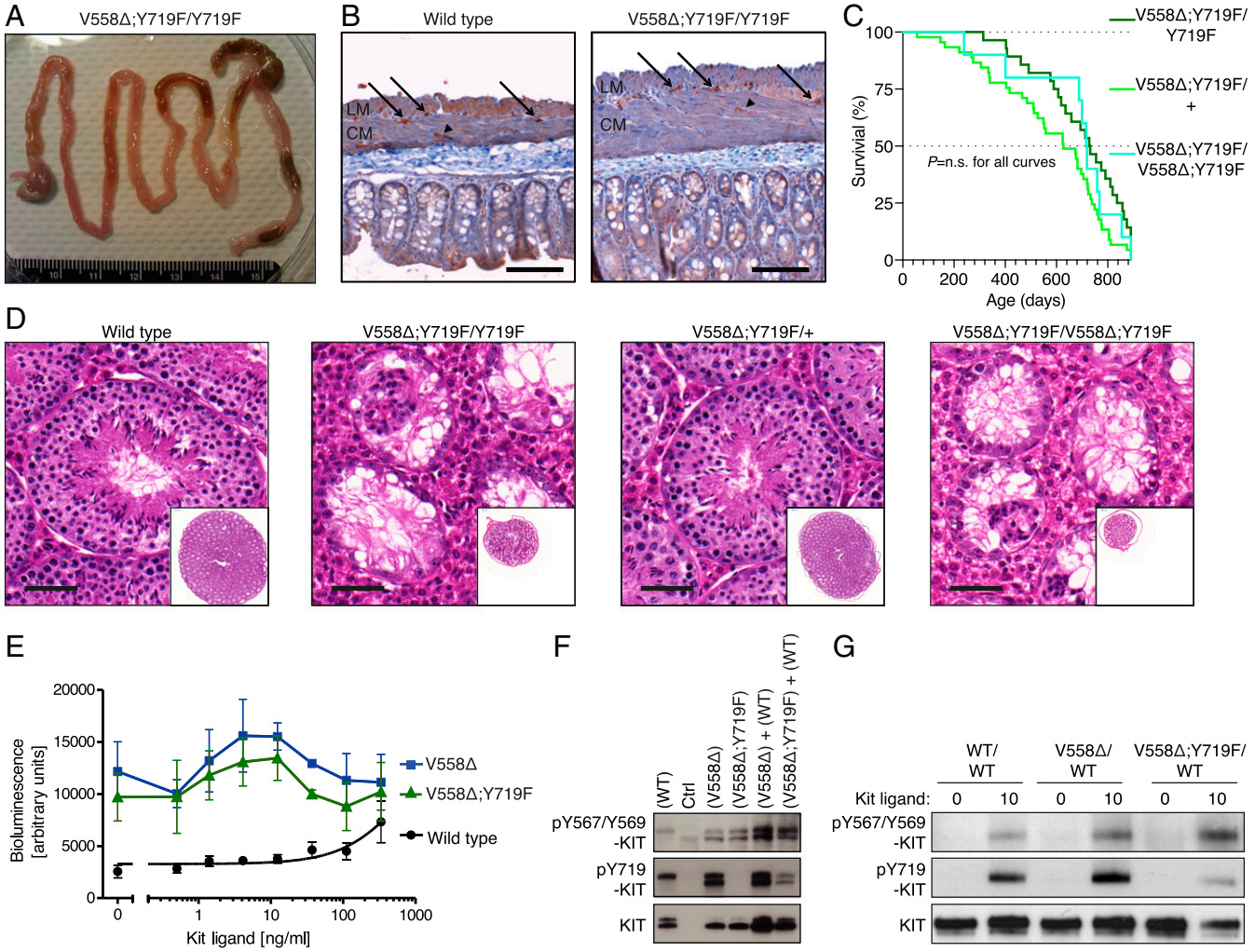

Fig. 3. Absence of tumorigenesis and impaired spermatogenesis in *Kit*$^{V558\Delta;Y719F/Y719F}$ mice, and functional kinase activity in mutant KIT$^{V558\Delta;Y719F}$ mice. (*A*) Gross pathology of the gastrointestinal tract of a 3-mo-old *Kit*$^{V558\Delta;Y719F/Y719F}$ mouse that appeared normal without cecal GIST, megaileum, or megacolon in comparison with *Kit*$^{V558\Delta/+}$ and *Kit*$^{V558\Delta;Y567F/Y567F}$ mice (10, 11) (Fig. 2*A*). (*B*) Immunohistochemical KIT staining of ICCs in cross-sections of the flat-mounted cecum from 7-mo-old WT and *Kit*$^{V558\Delta;Y719F/Y719F}$ mice (n = 14; 3–29 mo old). The typical presence and distribution of individual ICCs in the plane of the myenteric plexus (ICC-MY, arrow) between the circular (CM) and longitudinal (LM) muscle layers, as well as intramuscular ICC (ICC-IM; arrowhead), are preserved in *Kit*$^{V558\Delta;Y719F/Y719F}$ mice. Note the increased tissue surface in the right section due to the tangential cut of the sample, but the absence of ICC hyperplasia. n = 3. (Scale bar: 100 μm.) (*C*) Kaplan–Meier survival plot showing similar survival of *Kit*$^{V558\Delta;Y719F/Y719F}$, *Kit*$^{V558\Delta;Y719F/+}$, and *Kit*$^{V558\Delta;Y719F/V558\Delta;Y719F}$ mice. The median survival of *Kit*$^{V558\Delta;Y719F/Y719F}$ was 28 mo, as shown in Fig. 1. (*D*) Representative H&E-stained sections of testis showing normal morphology and spermatogenesis in 6-mo-old WT and *Kit*$^{V558\Delta;Y719F/+}$ mice and empty tubules in testis of 6-mo-old *Kit*$^{V558\Delta;Y719F/Y719F}$ and 3-mo-old *Kit*$^{V558\Delta;Y719F/V558\Delta;Y719F}$ mice. n = 3 each. (Scale bar: 50 μm.) (*E*) Kinase activity of WT KIT, KIT$^{V558\Delta}$, and KIT$^{V558\Delta;Y719F}$ mutants using the PathHunter eXpress receptor tyrosine kinase functional assay. Quantitative detection of β-gal activity (bioluminescence) is reported as arbitrary units. (*F*) Western blots from 293T cells transfected with control empty vector (Ctrl vector), WT *Kit*, *Kit*$^{V558\Delta}$, or *Kit*$^{V558\Delta;Y719F/Y719F}$ or cotransfected with *Kit*$^{V558\Delta}$ and WT or *Kit*$^{V558\Delta;Y719F/Y719F}$ and WT. (*G*) Immunoblot analysis of bone marrow-derived mast cell extracts from WT, *Kit*$^{V558\Delta/+}$, and *Kit*$^{V558\Delta;Y719F/+}$ mice. Antibodies specific for pKIT-Y567/Y569, pKIT-Y719, and KIT were used.

STAT3 phosphorylation without altering KIT expression (Fig. 2*E*, *a*, *d*, *g*, and *j*), consistent with our previous studies (11–13). In contrast, MAPK1/3 phosphorylation was at an intermediate level in untreated $Kit^{V558\Delta;Y567F/Y567F}$ tumors, indicating that SFK partially contributed to MAPK activation (Fig. 2*E*, *g–i*).

Western blot analysis further confirmed similar PI3K pathway activation in untreated $Kit^{V558\Delta;Y567F/Y567F}$ and $Kit^{V558\Delta/+}$ tumors, as demonstrated by phosphorylation of S6 and 4E-BP1 (Fig. 2 *F* and *G*). Again, phospho-MAPK1/3 (ERK1/2) was reduced in $Kit^{V558\Delta;Y567F/Y567F}$ tumors. SFK pathway activation was greatly reduced, as expected, but phospho-STAT3 was greatly reduced as well (Fig. 2 *F* and *G*). Taken together, our findings indicate that the oncogenic $Kit^{V558\Delta}$ mutation combined with the Kit^{Y567F} mutation did not affect PI3K signaling, but reduced the MAPK and STAT3 pathways and almost abrogated SFK activation.

Kit Kinase Is Functional in $Kit^{V558\Delta;Y719F/Y719F}$ Mice. The gastrointestinal tract in $Kit^{V558\Delta;Y719F/Y719F}$ mice appeared normal, with normal stomach, cecum, and colon morphology. KIT immunohistochemistry revealed normal morphology and density of myenteric and intramuscular ICCs (Figs. 1*C*, *j–l* and 3 *A* and *B*). The absence of GIST in $Kit^{V558\Delta;Y719F/Y719F}$ mice explained their normal lifespan (Fig. 1*B*). Remarkably, $Kit^{V558\Delta;Y719F/+}$ mice (harboring one WT *Kit* allele) also had a normal lifespan and did not develop GIST (Fig. 3*C*), which was surprising, given our assumption that mutant KIT protein could form heterodimers with WT KIT (KIT^{+}-$KIT^{V558\Delta;Y719F}$) and activate the PI3K moiety of WT KIT. Furthermore, $Kit^{V558\Delta;Y719F/V558\Delta;Y719F}$ mice homozygous for both mutations had an extended lifespan and failed to develop GIST. These results suggest that PI3K signaling is critical for GIST oncogenesis, and that even partial abrogation of PI3K recruitment to KIT is sufficient to prevent tumorigenesis, regardless of KIT oncogene dosage. Thus, PI3K may be a desirable candidate for pharmacologic targeting without the requirement for complete Kit inhibition.

While $Kit^{V558\Delta/+}$, $Kit^{V558\Delta;T669I/+}$, $Kit^{Y567F/Y567F}$, and $Kit^{V558\Delta;Y567F/Y567F}$ mice are fertile, $Kit^{Y719F/Y719F}$ mice showed a distinct blockage in spermatogenesis (24). Thus, we asked whether addition of the gain-of-function mutation $Kit^{V558\Delta}$ to the $Kit^{Y719F/Y719F}$ mutation might rescue azoospermia. We found that $Kit^{V558\Delta;Y719F/Y719F}$ mice recapitulated the testis phenotype of $Kit^{Y719F/Y719F}$ mice. Matings with multiple WT females over more than 6 mo did not produce offspring, testicular volume was reduced, and testis cross-sections revealed empty tubules (Fig. 3*D*). As was the case with survival, increasing the oncogenic dose in $Kit^{V558\Delta;Y719F/V558\Delta;Y719F}$ mice was not sufficient to compensate for the loss of KIT^{Y719}, indicating the need for at least one Y719 phosphorylation site for spermatogenesis. KIT is also known to have roles in hematopoiesis and mast cell development, and Kit mutant mice often present with a blood and/or mast cell phenotype. Skin mast cell numbers are increased in $Kit^{V558\Delta}$ mice, while $Kit^{V558\Delta;T669I/+}$ mice develop mast cell hyperplasia and microcytic erythrocytosis (10, 11). Nevertheless, in this study, the $Kit^{V558\Delta;Y719F/Y719F}$ mice had normal peripheral blood and skin mast cell levels.

Even though $Kit^{V558\Delta}$ is a potent oncogene and Kit^{Y719F} only affects PI3K activation in mice, we cannot exclude the possibility that when both $Kit^{V558\Delta}$ and Kit^{Y719F} mutations reside on the same allele, the protein does not fold properly, thereby inactivating KIT (10, 24). However, since $Kit^{V558\Delta;Y719F/Y719F}$ mice have normal ICCs and pigmentation, it is likely that KIT is functional. Given that *Kit*-null is perinatal lethal (27), the strongest in vivo evidence that this combination does not cause any severe KIT functional defects is our ability to derive viable adult mice homozygous for the $Kit^{V558\Delta;Y719F}$ allele. To confirm that the KIT kinase is functional in the $Kit^{V558\Delta;Y719F}$ mutation, we performed an in vitro kinase assay using cells expressing full-length KIT mutants. At baseline, without the addition of KIT ligand (KitL), $KIT^{V558\Delta;Y719F}$ kinase activity was significantly higher than WT KIT activity and similar to that of the $KIT^{V558\Delta}$ mutant (Fig. 3*E*). Both mutants were hypersensitive to increasing doses of KitL compared with WT KIT.

To further confirm that $KIT^{V558\Delta;Y719F}$ is functional, and to assess whether it is capable of canonical transphosphorylation, we transfected *Kit* constructs containing the WT, V558Δ, or V558Δ; Y719F mutations into 293T cells and measured KIT autophosphorylation by detection of specific KIT phosphotyrosine residues. The WT KIT receptor showed weak Y719 phosphorylation and barely detectable Y567/9 phosphorylation, similar to empty vector (Fig. 3*F*), consistent with the absence of KitL. The weak phosphorylation of Y719 was most likely due to KIT overexpression leading to random dimerization of receptors. In contrast, the $KIT^{V558\Delta}$ mutant had a net increase in both Y719 and Y567/9 phosphorylation, in accordance with its constitutive kinase activity. As expected, the $KIT^{V558\Delta;Y719F}$ mutant lacked Y719 phosphorylation, but exhibited levels of Y567 and Y569 phosphorylation comparable to those of the $KIT^{V558\Delta}$ mutant (Fig. 3*F*), indicating functional kinase activity of $KIT^{V558\Delta;Y719F}$. Cotransfection of $KIT^{V558\Delta;Y719F}$ with WT KIT showed weak phosphorylation of Y719 in addition to Y567/9, confirming that $KIT^{V558\Delta;Y719F}$ has canonical kinase activity in *trans*. In this combination, only WT KIT possessed a Y719 site, and its phosphorylation, at least the lower band, resulted from the presence of the mutant $KIT^{V558\Delta;Y719F}$, since Y719 phosphorylation of the lower band did not occur in the "WT-only" KIT lane.

To confirm that $KIT^{V558\Delta;Y719F}$ is functional when expressed at endogenous levels, primary cultures of bone marrow-derived mast cells (BMMCs) were derived from WT, $Kit^{V558/+}$, and $Kit^{V558\Delta;Y719F/+}$ mice (Fig. 3*G*). At baseline, the WT and mutant KIT proteins were barely phosphorylated at KIT^{Y719} and $KIT^{Y567/569}$. The addition of KitL increased phosphorylation to a greater degree in the mutants than in the WT, indicating that the mutants are hypersensitive to KitL stimulation and essentially confirming that the $KIT^{V558\Delta;Y719F}$ mutant protein is functional.

Taken together, these results indicate that the kinase in the $KIT^{V558\Delta;Y719F}$ mutant is functional and even constitutively active, like $KIT^{V558\Delta}$. Therefore, the absence of GIST in $Kit^{V558\Delta;Y719F/Y719F}$ mice is not due to a defect of the double-mutant KIT kinase, but rather must be explained by the lack of KIT pY719 signaling.

Response to Pharmacologic Inhibition of PI3K and MAPK in $Kit^{V558\Delta/+}$ Mice. Because PI3K signaling from KIT was required for GIST formation, we investigated whether selective pharmacologic inhibition of PI3K was effective against established tumors in $Kit^{V558\Delta/+}$ mice. We first tested the broadly acting dual PI3K/mTOR inhibitor voxtalisib (XL765). Tumor lysates from mice treated for 6 h showed decreased PI3K signaling, manifested by reductions in pAKT, pS6, and p4EBP1 (Fig. 4*A*). KIT and STAT3 phosphorylation were not affected, but, surprisingly, MAPK phosphorylation was increased. Seven days of treatment reduced tumor cell proliferation by 70% (Fig. 4*B*), although the histological response was minimal (Fig. 4*C*, *c*). To counteract MAPK activation by voxtalisib, we sought to use a MAPK inhibitor. The MEK inhibitor PD-325901 inhibited MAPK signaling without affecting PI3K and STAT signaling, but did not alter tumor proliferation (Fig. 4 *B* and *D*). Treatment with voxtalisib and PD325901 for 6 h reduced both PI3K and MAPK signaling, as well as phospho-STAT3 signaling (Fig. 4*E*). However, toxicity during 7 d of therapy required dosage reductions of both drugs to 5 mg/kg. Notably, low-dose voxtalisib and PD325901 therapy reduced tumor cell proliferation to a comparable degree as high-dose voxtalisib monotherapy (Fig. 4*B*), although the histological response was minimal (Fig. 4*C*, *d*). Taken together, these results indicate that targeting PI3K with the dual PI3K/mTOR inhibitor voxtalisib reduces tumor cell proliferation, but up-regulation of MAPK signaling might limit its efficacy.

The MAPK activation with voxtalisib therapy likely results from a feedback loop due to mTOR inhibition (28). Therefore, to avoid MAPK activation, we next assessed the pan-class I PI3K selective inhibitor pilaralisib (XL147), which does not inhibit mTOR and thus more closely resembles the genetic abrogation of PI3K signaling from KIT. Tumor lysates from $Kit^{V558\Delta/+}$ mice treated for

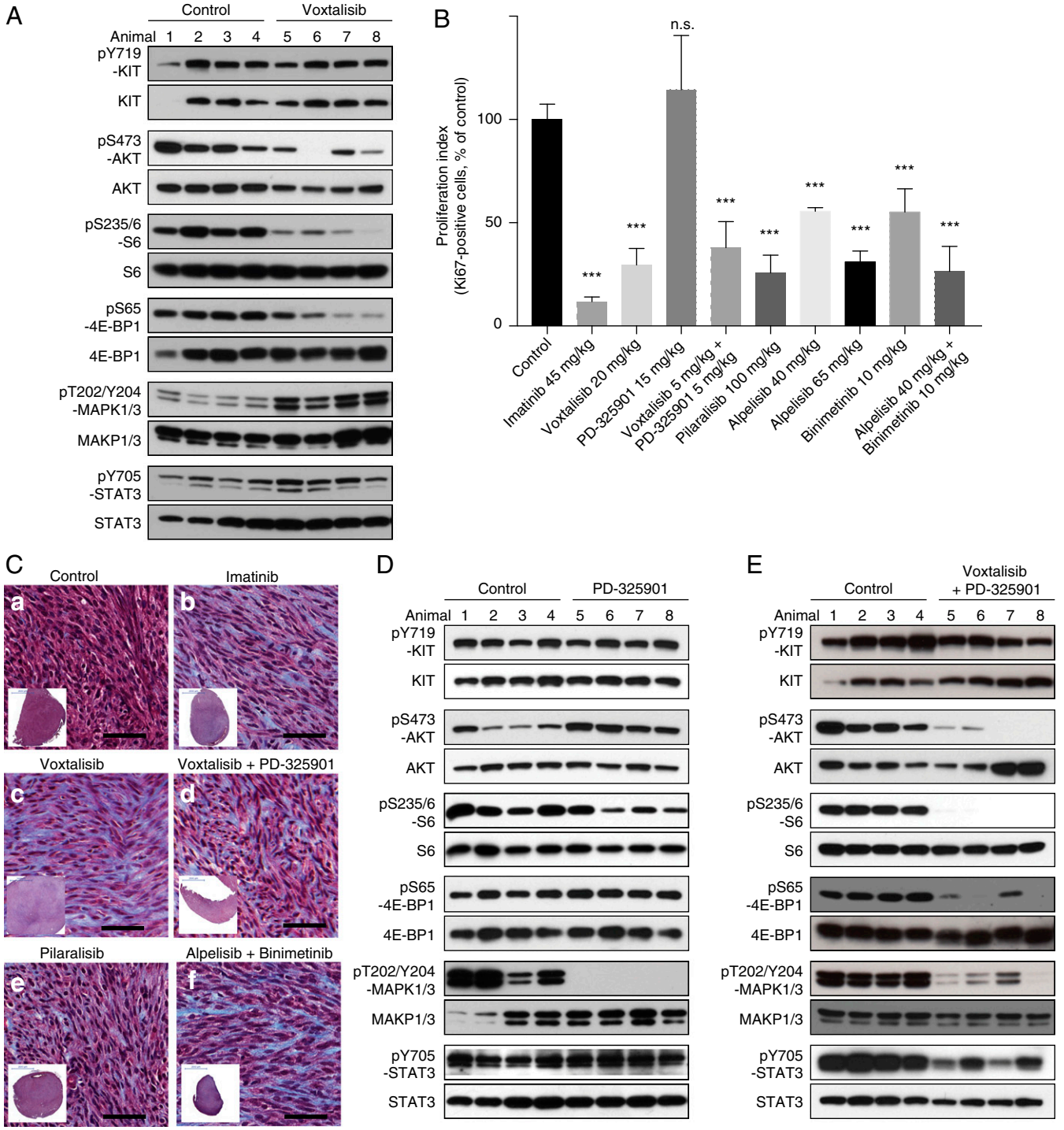

Fig. 4. PI3K and MAPK inhibition with the dual PI3K/mTOR inhibitor voxtalisib, the pan PI3K inhibitor pilaralisib, and the MEK inhibitor PD-325901 in $Kit^{V558\Delta/+}$ mice. (*A*) Immunoblot analysis of tumor extracts from $Kit^{V558\Delta}$ mice ($n = 4$/group) treated for 6 h with vehicle (Control) or voxtalisib (30 mg/kg). (*B*) Proliferation index measured by counting Ki-67–positive cells in GISTs from $Kit^{V558\Delta}$ mice treated as indicated. (*C*) Trichrome staining of GISTs from $Kit^{V558\Delta}$ mice treated for 7 d as indicated. Low-magnification overview of tumor section on bottom left corner. $n \geq 4$. The number of stained cells was assessed in at least three 250 × 250-μm nonoverlapping fields per tumor. Doses are specified in *Materials and Methods*. Note that due to toxicity, the dose of voxtalisib had to be reduced from 30 (mg/kg) to 20 (mg/kg) for the 7-d single treatment, and to 5 (mg/kg) for the 7-d combination treatment with PD-325901. (*D* and *E*) Immunoblot analysis of tumor extracts from $Kit^{V558\Delta/+}$ mice ($n = 4$/group) treated for 6 h with vehicle (Control) or 5 mg/kg (lanes 5 and 6) or 15 mg/kg (lanes 7 and 8) PD-325901 (*D*) or a combination of voxtalisib 30 mg/kg and 5 mg/kg PD-325901 (*E*).

4 h with pilaralisib showed decreased PI3K signaling with reduced pAKT, pS6, and p4EBP1 (Fig. 5*A*). In contrast, phosphorylated KIT, STAT3, and MAPK were unaffected (Fig. 5 *A* and *B*). IHC of tumors following 7 d of pilaralisib treatment revealed a lack of phosphorylated S6, no effect on MAPK1/3 or STAT3 activation (Fig. 5*C*), and reduced proliferation, yet only a minimal histological response (Fig. 4 *B* and *C*, *e*).

Because $Kit^{V558\Delta;Y567F/Y567F}$ tumors have less MAPK signaling and are smaller than $Kit^{V558\Delta/+}$ tumors, we reasoned that pilaralisib might be more effective if combined with a MAPK inhibitor. Thus, we treated $Kit^{V558\Delta/+}$ mice with the MEK inhibitor PD-325901 in addition to pilaralisib. After 6 h of treatment, PI3K and MAPK signaling were reduced, as was STAT3 signaling (Fig. 5*D*). Unfortunately, combination therapy was too toxic over 7 d of therapy.

Since voxtalisib and pilaralisib in combination with PD-325901 were not well tolerated, we evaluated other PI3K and MEK inhibitors. Alpelisib is a potent PIK3CA (PI3K-α) inhibitor, with minimal effects on PIK3CB (PI3K-β), PIK3CD (PI3K-δ), or PIK3CG (PI3K-γ). $Kit^{V558\Delta/+}$ mice treated for 7 d with alpelisib had decreased PI3K signaling with reduced pAKT, pS6, and p4EBP1, while KIT, MAPK, and STAT3 activation were unchanged (Fig. 6*A*). Mice treated for 7 d with the ATP noncompetitive MEK inhibitor binimetinib had less pMAPK1/3 (Fig. 6*B*). pSTAT3 was also reduced, but PI3K signaling was unaltered. The combination of alpelisib and binimetinib was well tolerated and reduced PI3K pathway activation, pMAPK1/3, and pSTAT3 (Fig. 6*C*). Furthermore, tumor cell proliferation was reduced by 75%, while the histological response was slightly improved (Fig. 4 *B* and *C*, *f*).

Imatinib-Resistant $Kit^{V558\Delta;T669I/+}$ Tumors Respond to Dual PI3K and MEK Inhibition. Since alpelisib and binimetinib were found to target two major signaling pathways downstream of KIT and to lack toxicity in $Kit^{V558\Delta/+}$ mice, we evaluated whether they could be used in combination to overcome imatinib resistance. For this purpose, imatinib-resistant $Kit^{V558\Delta;T669I/+}$ mice (11) were treated for 7 d with alpelisib and binimetinib. Both PI3K and MAPK signaling were reduced, as was tumor cell proliferation (Fig. 7 *A* and *B*). Furthermore, the histological response was increased (Fig. 7*C*). Thus, targeting downstream components of KIT signaling was also effective in the setting of imatinib resistance.

Discussion

Here we engineered double-mutant mice carrying both the oncogenic $Kit^{V558\Delta}$ mutation and the Kit^{V567F} or the Kit^{Y719F} mutation on the same allele. Mice carrying the $Kit^{V558\Delta;567F}$ allele developed smaller GIST lesions than the $Kit^{V558\Delta}$ mutant mice, indicating that signal transducers that bind to KIT^{Y567} have a role in tumor growth. By crossing $Kit^{V558\Delta;567F/+}$ mice with our previously developed single-mutant $Kit^{Y567F/+}$ mice, we generated double-mutant compound heterozygous $Kit^{V558\Delta;Y567F/Y567F}$ mice that are homozygous for the Y567F mutation, to ensure that any signal that normally emanates from phospho-Y567 is abrogated. SFK activation was dramatically impaired in GIST of the $Kit^{V558\Delta;Y567F/Y567F}$ mice compared with the $Kit^{V558\Delta/+}$ mice. This is consistent with an important role for SFKs in KIT-mediated activation of the RAS/MAPK pathway (15). In addition, we observed a partial reduction in STAT3 signaling in tumors of $Kit^{V558\Delta;Y567F/Y567F}$ mice (29). In mast cell/myeloid cell transformation by oncogenic Kit, Y567F mutation accelerated tumorigenesis, presumably due to inhibited activation of SHIP1,

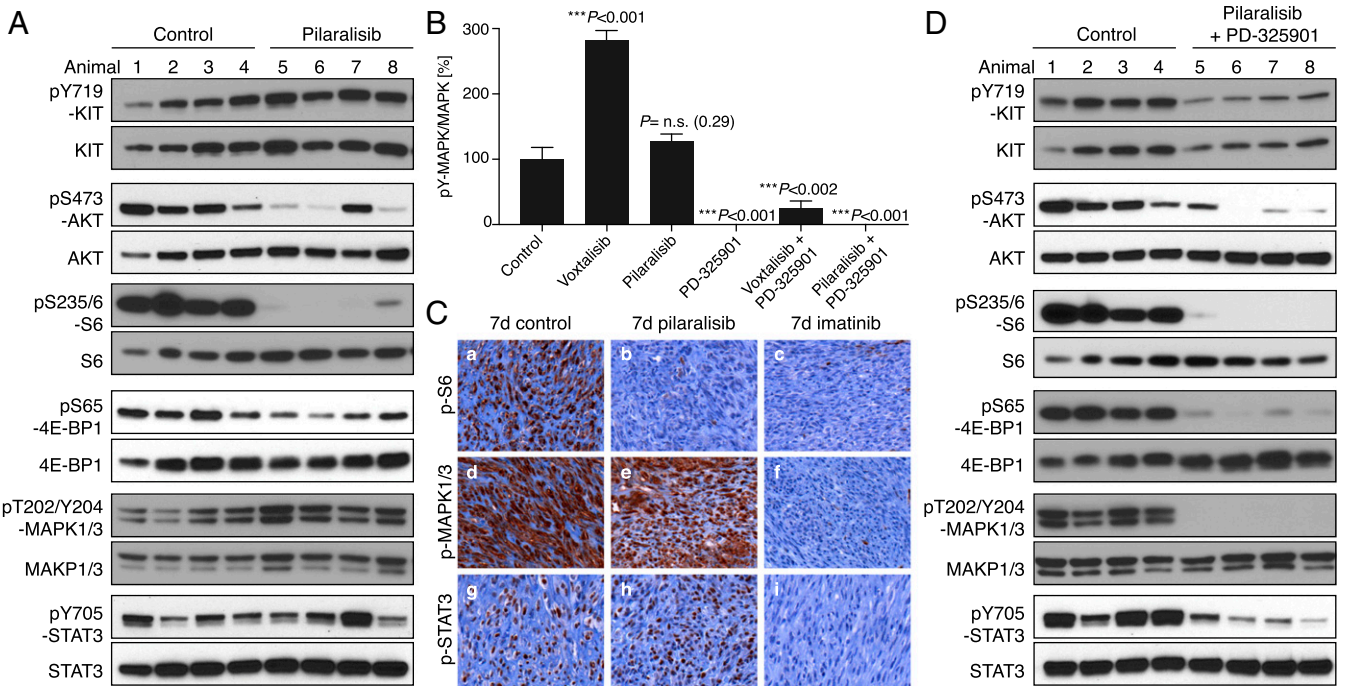

Fig. 5. Inhibition of PI3K resulted in a significant reduction in GIST proliferation. $Kit^{V558\Delta/+}$ mice (n = 4/group) were treated for 4 h (*A*) with pilaralisib (100 mg/kg) alone, (*B*) with PD-325901 (15 mg/kg) alone, and (*D*) with both pilaralisib (100 mg/kg) and PD-325901 (15 mg/kg) and analyzed by immunoblotting. (*B*) Comparison of the level of activation of phospho-MAPK1/3 in GIST from mice treated with voxtalisib and pilaralisib alone or in combination with PD-325901. The level of activation of phospho-MAPK1/3 was determined by densitometry analysis of the respective bands from Western blots and measured as the ratio of phospho/total for each protein compared with control. The scale is arbitrary units (intensity of gray shading). (*C*) Representative results of IHC analysis of GIST after long-term (7 d) treatment of $Kit^{V558\Delta/+}$ mice with vehicle (control), pilaralisib, or imatinib. As a positive control for IHC, imatinib down-regulated all three signaling readouts—p-MAPK, pS6, and p-STAT3—as reported previously (11). Antibodies used are specific for pS6 (*a*–*c*), p-MAPK1/3 (*d*–*f*), and p-STAT3 (*g*–*i*) on 5-μm sections of GISTs. Tumor sections from the different treatment groups ($n \geq 3$ animals each) were placed next to each other on the same microscope slide to enable cross-comparison of staining intensities (40× objective).

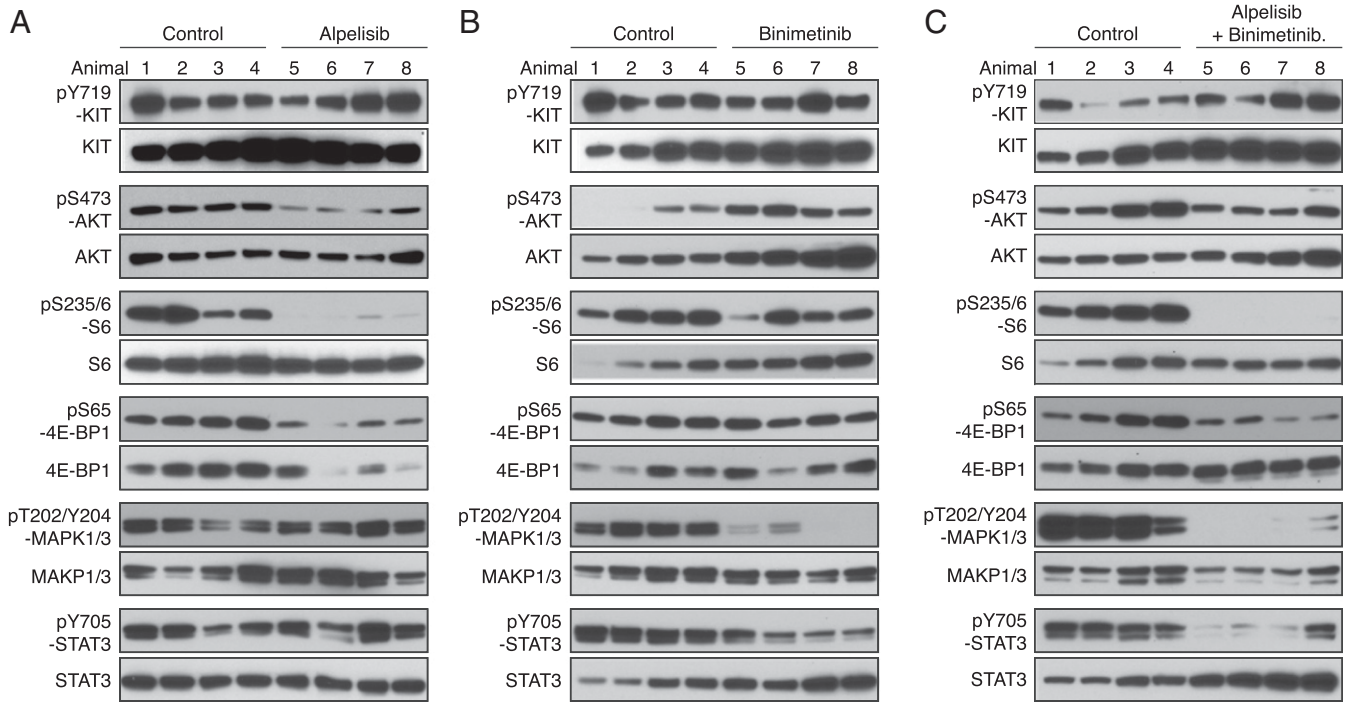

Fig. 6. PI3K-alpha inhibition by alpelisib in $Kit^{V558\Delta/+}$ mice. Immunoblot analysis of tumor extracts from $Kit^{V558\Delta/+}$ mice (n = 4/group) treated for 4 h with alpelisib 20 mg/kg (*A*), binimetinib 3.5 mg/kg (*B*), or both alpelisib 20 mg/kg and binimetinib 3.5 mg/kg (*C*) compared with vehicle (control).

a hematopoietic-specific negative regulator of PI3K (14, 17, 30). In contrast, in $Kit^{V558\Delta;Y567F/Y567F}$ mice, the Y567F mutation diminished tumorigenesis, indicating that KIT^{pY567} is a positive regulator of tumorigenesis in GIST. Since a mild hematopoietic pro-B/pro T-cell phenotype in $KIT^{Y567F/Y567F}$ mutant mice becomes apparent after age 8 mo, biochemical analysis of tumor tissue was performed in tumors from 3- to 4-mo-old mice (20, 22).

Importantly, our results provide in vivo evidence that the direct activation of the PI3K-pathway via KIT^{Y719} is required for GIST tumorigenesis. The KIT^{Y719} phosphorylation site also has been postulated to be of importance in myeloproliferative disease induced by the kinase domain mutation KIT^{D814V} (human KIT^{D816V}), based on experiments with chimeric proteins consisting of the extracellular domain of human M-CSFR and the intracellular domain of murine KIT (18, 31). We considered the possibility of defective ICC development in $Kit^{V558\Delta;Y719F/Y719F}$ mice, which would readily explain the absence of hyperplasia and tumor development, as ICCs or their progenitors are the presumed cells of origin of GIST (32). However, ICCs developed normally and stained positive for KIT. In addition, the kinase activity of the $KIT^{V558\Delta;Y719F}$ protein was not impaired, strengthening the idea that disruption of PI3K signaling is responsible for the lack of tumor development. The mutant KIT alleles were expressed under the control of the endogenous Kit transcription machinery and thus expressed continuously during ICC development; that is, the experiments did not distinguish whether the phenotypes derived were due to a failure in tumor initiation or a failure in maintaining an oncogenic state. Also, $Kit^{V558\Delta;Y719F/Y719F}$ mice lacked the PI3K-binding site in all KIT-expressing cells starting at fertilization. Thus, we cannot rule out that the absence of tumorigenesis in our model could be the result of a defect in tumor initiation.

In addition, it is possible that proteins other than PI3K-family members are being recruited to the phospho-KIT^{Y719} site and are necessary for transformation. Nevertheless, pharmacologic inhibitors of the PI3K pathway in tumor-bearing $Kit^{V558\Delta/+}$ mice, including the dual PI3K/mTOR inhibitor voxtalisib, the pan-PI3K inhibitor pilaralisib, and the PI3K-alpha–restricted inhibitor alpelisib, each diminished tumor proliferation, indicating that PI3 kinase makes a major contribution to tumor cell proliferation in established GIST. The presumed selectivity of these inhibitors for PI3K was generally confirmed in our mice, since phosphorylation of S6 kinase and 4EBP1 were inhibited, while MAPK and STAT3 activation were unaffected. The dual PI3K/mTOR inhibitor voxtalisib increased MAPK activation in GIST. This is consistent with reports that mTORC1 inhibition promotes MAPK activation in a mouse model of prostate cancer and in patients with metastatic disease subjected to mTOR inhibition therapy (28). The feedback

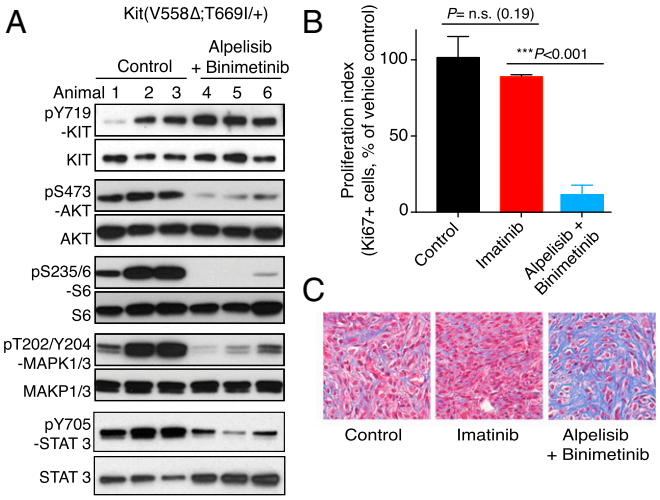

Fig. 7. GISTs from imatinib-resistant $Kit^{V558\Delta;T669I/+}$ mice respond to combined PI3K and MAPK inhibition. $Kit^{V558\Delta;T669I/+}$ mice (n = 3/group) were treated for 7 d with vehicle (Control), imatinib, or alpelisib (40 mg/kg) and binimetinib (10 mg/kg) and analyzed by immunoblotting (*A*), proliferation index (*B*), and Trichrome staining (*C*).

activation of MAPK with voxtalisib provided a rationale for using an MEK inhibitor in combination with a PI3K inhibitor.

In contrast to mice carrying the $Kit^{V558\Delta;Y719F/Y719F}$ double mutation, mice carrying a $Kit^{V558\Delta;Y567F/Y567F}$ double mutation developed GIST, although tumor development was attenuated and the animals had an extended lifespan. In these animals, PI3K signaling was not affected, but SFK pathway activation was strongly diminished, and phospho-MAPK1/3 and phospho-STAT3 were reduced as well. In agreement with those observations, treatment of $Kit^{V558\Delta/+}$ mice with the MEK inhibitors PD-325901 or binimetinib diminished MAPK1/3 and STAT3 phosphorylation/activation. These findings indicate a requirement for the direct engagement of distinct pathways by KIT for full tumor growth. Thus, dual inhibition of both the PI3K and MAPK branches in oncogenic KIT signaling was pursued. Whereas combination treatment with either voxtalisib plus PD-325901 or pilaralisib plus PD-325901 was too toxic, combination treatment with the PI3K-alpha inhibitor alpelisib and the MAPK inhibitor binimetinib was tolerated and shows promise for use in patients with GIST, particularly those with imatinib-resistant GIST, as demonstrated in imatinib-resistant gatekeeper $Kit^{V558\Delta;T669I/+}$ mice. PI3K inhibitors alone and in combination with imatinib have shown antitumor effects in GIST xenograft models; however, the most common imatinib-resistant GIST mutations (KIT exons 11–13 and 11–14) have not been tested (33, 34). Targeting of the PI3K pathway with the AKT inhibitor MK-2206 has been shown to increase imatinib efficacy in cell culture and in xenografts with imatinib-sensitive and -resistant GIST cell lines (35). Our studies with immunocompetent mice carrying either the $Kit^{V558\Delta}$ or the common KIT imatinib-resistant gatekeeper mutation strengthen our argument that the combination of PI3K and MEK inhibition could be beneficial for treating patients with imatinib-resistant GIST.

In summary, our results suggest that a detailed analysis of distinct oncogenic signaling pathways mediated by oncogenic tyrosine kinases in specific cellular contexts may lead to new and improved treatment strategies.

Materials and Methods

Generation of Mouse Strains. The V558Δ mutation was introduced by site-directed mutagenesis into a 2.1-kb EcoRI/MluI fragment across *Kit* exons 9–11 from a 129/SvJ mouse library (24) serving as the 5′ homology arm of the targeting vector. For the $Kit^{V558\Delta;Y567F}$ allele, the Y567F mutation was introduced into the same 5′ arm for homologous recombination (HR) (Fig. S1). The 5′ HR arm was linked 3′ to a floxed neomycin-resistance (NEO) gene expression cassette. The 3′ HR arm for the $Kit^{V558\Delta;Y567F}$ allele was a 1.3-kb MluI/BsrGI-NcoI fragment across exons 12–13 (Fig. S1). For the $Kit^{V558\Delta;Y719F}$ allele, this arm was elongated by the 3′ directly neighboring 129/SvJ genomic DNA, a 2.1-kb BsrGI-NcoI/BamHI fragment including exon 14, and a 3.8-kb BamHI fragment across exons 15–17 including the Y719F mutation in exon 15. The final targeting vector was completely sequenced before linearization and electroporation into CJ7 ES cells (36).

Screening of BamHI-digested genomic DNA from 288 ES cell clones each by Southern blot analysis with a 3′ external probe across *Kit* exon 14 or a 5′ external probe across *Kit* exon 8 yielded 17 (5.9%) and 19 (6.6%) positive clones for the $Kit^{V558\Delta;Y567F}$ and $Kit^{V558\Delta;Y719F}$ projects, respectively. Four ES cell clones carried both the V558Δ mutation and the nearby Y567F mutation, and two clones carried both the V558Δ mutation and the distant Y719F mutation, respectively, as assessed by sequencing, and showed a normal karyotype. C57BL/6J blastocyst injections of two of these clones each gave rise to 19/21 high-grade chimeras (>90% agouti coat color), one each of which gave germ line transmission of the double mutations. After crossing to C57BL/6J mice, in all agouti F1 animals heterozygous for the NEO allele, the presence of the V558Δ;Y56F and V558Δ;Y719F mutations, and the integrity of both loxP sites was confirmed by sequencing. To remove the floxed NEO cassette, F1 $Kit^{V558\Delta;Y567F\text{-}NEO/+}$ and $Kit^{V558\Delta;Y719F\text{-}NEO/+}$ males were bred to B6.FVB-Tg(EIIa-cre) C5379Lmgd/J females (The Jackson Laboratory).

Genotyping PCR was performed across the original intron 11 MluI site, which was replaced by a 134-bp loxP scar in the case of the targeted alleles. Of the two resulting fragments (WT allele, 643 bp; targeted allele, 777 bp), the longer one was isolated by gel purification, and the integrity of the V558Δ mutation (and in case of the $Kit^{V558\Delta;Y567F}$ allele, of the adjacent Y567F mutation), as well as of the remaining loxP site, was confirmed by sequencing. Only $Kit^{V558\Delta;Y567F/+}$ and $Kit^{V558\Delta;Y719F/+}$ animals that genotyped negative for the Cre allele were used for subsequent backcrosses to $Kit^{Y567F/Y567F}$ (20) and $Kit^{Y719F/+}$ mice (24), respectively, which had been backcrossed onto the C57BL/6J background for at least 10 generations previously. To produce $Kit^{V558\Delta;Y567F/567}$ mice, $Kit^{V558\Delta;Y567F/+}$ mice were intercrossed with $Kit^{Y567F/Y567F}$ mice, and to produce $Kit^{V558\Delta;Y719F/719}$ mice, $Kit^{V558\Delta;Y719F/+}$ mice were intercrossed with $Kit^{Y719F/+}$ mice, because $Kit^{Y719F/Y719F}$ mice are sterile (24). A PCR strategy bracketing the 134-bp loxP scar was used for routine genotyping thereafter (WT allele, 291 bp; targeted allele, 425 bp) with the primers mKitEx11F, 5′-CATAGACCCGACGCAACTTC-3′, and mKitIn11R, 5′-GGTTCCCAAATCAACAAGGC-3′. Initial experiments were done with backcross generation N3, and repetitions were done with generation N4–N10+ animals. No change in phenotype was observed in different backcross generations. $Kit^{V558\Delta/+}$ and $Kit^{V558\Delta;T669I/+}$ mice have been described previously (10, 11). All animal procedures were approved by the Institutional Animal Care and Use Committee of Memorial Sloan Kettering Cancer Center.

Receptor Tyrosine Kinase Functional Assay. This assay was performed using the PathHunter eXpress Receptor Tyrosine Kinase Assay Kit (DiscoveRx), following the manufacturer's instructions. Custom-made U2OS cells expressing the large β-gal subunit fused to the SH2 domain of phospholipase Cγ (PLCγ) (enzyme acceptor) transiently expressing murine cDNA of *Kit-WT*, *Kit-V558Δ*, or *Kit-V558Δ*;Y719F were C-terminally tagged with a small β-gal subunit (ProLink tag) to assay full-length KIT functional autophosphorylation on tyrosine recruiting PLCγ (Y728), which is immediately adjacent to the PI3K recruitment site affected by the KIT^{Y719} mutation. Ligand and/or mutation activation of the KIT receptor causes its autophosphorylation and subsequent binding of PLCγ to KIT^{PY728}, resulting in complementation of the two fragments of β-gal and formation of a functional enzyme. β-gal activity was then quantitatively detected using the chemiluminescent substrate in the PathHunter Kit.

Western Blot Analysis. Tumor lysates were prepared as described previously (13) with the following modifications. Snap-frozen tumor was first homogenized in a PowerGen 1000 homogenizer (Thermo Fisher Scientific) and then incubated on ice for 30 min. Lysates were cleared by centrifugation at 4 °C for 30 min and then fractionated by SDS/PAGE. Protein extracts were prepared from tumors of several mice to assess individual variability in the response to drugs. Proteins were visualized by Western blot analysis after incubation with appropriate antibodies. Phospho-KIT (Tyr719), KIT, Phospho-p44/42 MAPK (Thr202/Tyr204), p44/42 MAPKinase, phospho-S6 protein (Ser235/236), S6 protein, phospho-AKT (Ser473), AKT, phospho-STAT3 (Tyr705), STAT3, phospho-STAT5 (Tyr694), STAT5, phospho-SRC family (Tyr416), and SRC were obtained from Cell Signaling Technology. Phospho-KIT (Tyr568 + Tyr569) was obtained from Abcam.

Drug Treatment in Mice. Mice were maintained in a specific pathogen-free animal facility and used in accordance with an institutional approved protocol. Voxtalisib (XL765) and pilaralisib (XL147) were provided by Exelixis. Voxtalisib was suspended at 2 mg/mL in water/10 mM HCl. For the 6-h treatment, voxtalisib was administered once at 30 mg/kg by gavage. For the 7-d treatment, it was administered at 20 mg/kg by gavage twice a day (30 mg/kg was toxic). PD325901 was administered by gavage, once at 5 or 15 mg/kg for the 6-h treatment and once a day at 15 mg/kg for the 7-d treatment. For combination treatment with voxtalisib and PD325901, the dose had to be reduced to 5 mg/kg each and administered only once daily. Pilaralisib was solubilized in water, sonicated and administered at 100 mg/kg by gavage within 60min of formulation. It was administered once for the 4-h treatment, and once a day for the 7-d treatment. For combination treatment, pilaralisib and PD325901 were administered daily at 100 mg/kg and 15 mg/kg, respectively. Alpelisib (37) and binimetinib (38) were suspended at 4 mg/mL in 0.5% Tween 80 and 1% carboxymethyl cellulose in water. Alpelisib was administered at 20 mg/kg (Western blots), 40 mg/kg (Ki-67 and trichrome), or 65 (Ki-67) mg/kg by gavage once daily for 7 d. Binimetinib was administered at 3.5 mg/kg (Western blots) or 10 mg/kg (Ki-67 and trichrome) by gavage twice daily for 7 d. For combination treatment, alpelisib and binimetinib were administered for 7 d at 20 mg/kg (once daily) and 3.5 mg/kg (twice daily), respectively (Western blots) or at 40 mg/kg (once daily) and 10 mg/kg (twice daily), respectively (Ki-67 and trichrome). Imatinib mesylate (Novartis) was suspended in water and injected i.p. twice daily at 45 mg/kg. Sunitinib malate (LC Laboratories) was solubilized freshly in 30% Cremophor EL (Sigma-Aldrich), 30% polyethylene glycol 400, 10% ethanol, and 10% glucose every 4 d and was administered at 40 mg/kg once daily by gavage.

The same formulation without sunitinib was used as vehicle control for the treatments shown in Fig. 5.

Histological and Immunohistochemical Analyses. Microscopic and IHC analyses were performed as described previously (13). Given the differing pharmacokinetic and pharmacodynamic profiles of the drugs used, treated mice were dissected for histological and IHC analyses on the following schedule: for imatinib, sunitinib, PD325901, and respective vehicle-treated animals, 6 h after the last injection; for voxtalisib, 5 h after the last injection; and for pilaralisb, alpelisib, and binimetinib, 4 h after the last injection. Tumors were immediately frozen in liquid nitrogen and/or fixed in fresh 4% paraformaldehyde rotating at 4 °C overnight. After paraffin embedding, 5-μm sections of the tumors of at least three different animals per treatment group and of at least three different treatments were placed on microscopic slides next to one another to enable cross-comparison within a slide after IHC staining with the antibodies indicated. Antibodies used were Phospho(P)-ribosomal protein S6 (S235/236) (D57.2.2E), P-MAPK (ERK-1/2) (T202/204) (20G11), P-STAT3 (Y705) (D3A7), and cleaved caspase-3 (CC3, Asp175, 9961), all from Cell Signaling Technology; Ki-67 (Vector Laboratories); and KIT (Oncogene Science). Stained slides were scanned with a MIRAX slide scanner (Carl Zeiss) and Ki-67 staining was quantified by counting stained nuclei in nine 250 × 250 μm fields of at least three different tumors per genotype and treatment. Tissues for H&E staining were fixed in 10% neutral buffered formalin and embedded in paraffin; 5-μm sections were stained with H&E for histological analysis.

Statistical Analysis. Statistical analysis was performed with GraphPad Prism version 5.0. Comparisons between two groups was done by unpaired *t* test analysis assuming unequal variances using GraphPad Prism. Statistical significance was achieved when $P < 0.05$.

ACKNOWLEDGMENTS. We thank Willie Mark and Antoinette Rookard from the Mouse Genetics Core facility for help with gene targeting experiments; Mesru Turkekul, Asfar Barlas, and Ning Fan from the Molecular Cytology core facility at Memorial Sloan Kettering Cancer Center for help with histological analysis; Peterson Chao and Adriana Guevara for assistance with experiments; and Russell Holmes and John Burrowes for logistical and administrative support. This study was supported by the National Institutes of Health (Grants R01 HL55748, to P.B.; CA102774, to P.B.; P50 CA140146, to P.B. and C.R.A.; R01 CA102613, to R.P.D.; and P30 CA008748) and the Starr Cancer Consortium (P.B. and C.R.A.).

1. Hirota S, et al. (1998) Gain-of-function mutations of c-kit in human gastrointestinal stromal tumors. *Science* 279:577–580.
2. Lorincz A, et al. (2008) Progenitors of interstitial cells of Cajal in the postnatal murine stomach. *Gastroenterology* 134:1083–1093.
3. Huizinga JD, et al. (1995) W/kit gene required for interstitial cells of Cajal and for intestinal pacemaker activity. *Nature* 373:347–349.
4. Maeda H, et al. (1992) Requirement of c-kit for development of intestinal pacemaker system. *Development* 116:369–375.
5. Demattео RP, et al. (2009) Adjuvant imatinib mesylate after resection of localised, primary gastrointestinal stromal tumour: A randomised, double-blind, placebo-controlled trial. *Lancet* 373:1097–1104.
6. Blanke CD, et al. (2008) Long-term results from a randomized phase II trial of standard- versus higher-dose imatinib mesylate for patients with unresectable or metastatic gastrointestinal stromal tumors expressing KIT. *J Clin Oncol* 26:620–625.
7. Antonescu CR, et al. (2005) Acquired resistance to imatinib in gastrointestinal stromal tumor occurs through secondary gene mutation. *Clin Cancer Res* 11:4182–4190.
8. Tamborini E, et al. (2004) A new mutation in the KIT ATP pocket causes acquired resistance to imatinib in a gastrointestinal stromal tumor patient. *Gastroenterology* 127:294–299.
9. Nishida T, et al. (1998) Familial gastrointestinal stromal tumours with germline mutation of the KIT gene. *Nat Genet* 19:323–324.
10. Sommer G, et al. (2003) Gastrointestinal stromal tumors in a mouse model by targeted mutation of the Kit receptor tyrosine kinase. *Proc Natl Acad Sci USA* 100: 6706–6711.
11. Bosbach B, et al. (2012) Imatinib resistance and microcytic erythrocytosis in a KitV558Delta;T669I/+ gatekeeper-mutant mouse model of gastrointestinal stromal tumor. *Proc Natl Acad Sci USA* 109:E2276–E2283.
12. Rossi F, et al. (2006) Oncogenic Kit signaling and therapeutic intervention in a mouse model of gastrointestinal stromal tumor. *Proc Natl Acad Sci USA* 103:12843–12848.
13. Rossi F, et al. (2010) Imatinib up-regulates compensatory integrin signaling in a mouse model of gastrointestinal stromal tumor and is more effective when combined with dasatinib. *Mol Cancer Res* 8:1271–1283.
14. Huber M, et al. (1998) Targeted disruption of SHIP leads to Steel factor-induced degranulation of mast cells. *EMBO J* 17:7311–7319.
15. Lennartsson J, et al. (1999) Phosphorylation of Shc by Src family kinases is necessary for stem cell factor receptor/c-kit–mediated activation of the Ras/MAP kinase pathway and c-fos induction. *Oncogene* 18:5546–5553.
16. Timokhina I, Kissel H, Stella G, Besmer P (1998) Kit signaling through PI 3-kinase and Src kinase pathways: An essential role for Rac1 and JNK activation in mast cell proliferation. *EMBO J* 17:6250–6262.
17. Chaix A, et al. (2014) KIT-D816V oncogenic activity is controlled by the juxtamembrane docking site Y568-Y570. *Oncogene* 33:872–881.
18. Mali RS, et al. (2012) Role of SHP2 phosphatase in KIT-induced transformation: Identification of SHP2 as a druggable target in diseases involving oncogenic KIT. *Blood* 120:2669–2678.
19. Serve H, Hsu YC, Besmer P (1994) Tyrosine residue 719 of the c-kit receptor is essential for binding of the P85 subunit of phosphatidylinositol (PI) 3-kinase and for c-kit-associated PI 3-kinase activity in COS-1 cells. *J Biol Chem* 269:6026–6030.
20. Agosti V, et al. (2004) Critical role for Kit-mediated Src kinase but not PI 3-kinase signaling in pro T and pro B cell development. *J Exp Med* 199:867–878.
21. Agosti V, Karur V, Sathyanarayana P, Besmer P, Wojchowski DM (2009) A KIT juxtamembrane PY567 -directed pathway provides nonredundant signals for erythroid progenitor cell development and stress erythropoiesis. *Exp Hematol* 37:159–171.
22. Kimura Y, et al. (2004) Targeted mutations of the juxtamembrane tyrosines in the Kit receptor tyrosine kinase selectively affect multiple cell lineages. *Proc Natl Acad Sci USA* 101:6015–6020.
23. Blume-Jensen P, et al. (2000) Kit/stem cell factor receptor-induced activation of phosphatidylinositol 3′-kinase is essential for male fertility. *Nat Genet* 24:157–162.
24. Kissel H, et al. (2000) Point mutation in kit receptor tyrosine kinase reveals essential roles for kit signaling in spermatogenesis and oogenesis without affecting other kit responses. *EMBO J* 19:1312–1326.
25. John GB, Shidler MJ, Besmer P, Castrillon DH (2009) Kit signaling via PI3K promotes ovarian follicle maturation but is dispensable for primordial follicle activation. *Dev Biol* 331:292–299.
26. Gibbons SJ, et al. (2003) Kit/stem cell factor receptor-induced phosphatidylinositol 3′-kinase signalling is not required for normal development and function of interstitial cells of Cajal in mouse gastrointestinal tract. *Neurogastroenterol Motil* 15:643–653.
27. Russell ES (1979) Hereditary anemias of the mouse: A review for geneticists. *Adv Genet* 20:357–459.
28. Carracedo A, et al. (2008) Inhibition of mTORC1 leads to MAPK pathway activation through a PI3K-dependent feedback loop in human cancer. *J Clin Invest* 118:3065–3074.
29. Chaix A, et al. (2011) Mechanisms of STAT protein activation by oncogenic KIT mutants in neoplastic mast cells. *J Biol Chem* 286:5956–5966.
30. Ma P, et al. (2011) Balanced interactions between Lyn, the p85alpha regulatory subunit of class I(A) phosphatidylinositol-3-kinase, and SHIP are essential for mast cell growth and maturation. *Mol Cell Biol* 31:4052–4062.
31. Ma P, et al. (2012) Role of intracellular tyrosines in activating KIT-induced myeloproliferative disease. *Leukemia* 26:1499–1506.
32. Kwon JG, et al. (2009) Changes in the structure and function of ICC networks in ICC hyperplasia and gastrointestinal stromal tumors. *Gastroenterology* 136:630–639.
33. Floris G, et al. (2013) A potent combination of the novel PI3K inhibitor, GDC-0941, with imatinib in gastrointestinal stromal tumor xenografts: Long-lasting responses after treatment withdrawal. *Clin Cancer Res* 19:620–630.
34. Van Looy T, et al. (2014) Phosphoinositide 3-kinase inhibitors combined with imatinib in patient-derived xenograft models of gastrointestinal stromal tumors: Rationale and efficacy. *Clin Cancer Res* 20:6071–6082.
35. Zook P, et al. (2017) Combination of imatinib mesylate and AKT inhibitor provides synergistic effects in preclinical study of gastrointestinal stromal tumor. *Clin Cancer Res* 23:171–180.
36. Swiatek PJ, Gridley T (1993) Perinatal lethality and defects in hindbrain development in mice homozygous for a targeted mutation of the zinc finger gene Krox20. *Genes Dev* 7:2071–2084.
37. Fritsch C, et al. (2014) Characterization of the novel and specific PI3Kalpha inhibitor NVP-BYL719 and development of the patient stratification strategy for clinical trials. *Mol Cancer Ther* 13:1117–1129.
38. Chen X, et al. (2014) Combined PKC and MEK inhibition in uveal melanoma with GNAQ and GNA11 mutations. *Oncogene* 33:4724–4734.